Supporting Information

Ion Desorption Efficiency and Internal Energy Transfer in Carbon-Based Surface-Assisted Laser Desorption/Ionization Mass Spectrometry: Desorption Mechanism(s) and the Design of SALDI Substrates

Ho-Wai Tang, Kwan-Ming Ng*, Wei Lu and Chi-Ming Che*

Department of Chemistry and Open Laboratory of Chemical Biology of the Institute of Molecular Technology for Drug Discovery and Synthesis, The University of Hong Kong, Pokfulam Road, Hong Kong SAR

* **To whom correspondence should be addressed:**
K.-M. Ng
Fax: (852) 2857 1586
E-mail: kwanmng@hku.hk

Co-correspondence:
C.-M. Che
Fax: (852) 2857 1586
E-mail: cmche@hku.hk

Description of the Delayed Extraction Method (DE method) for Measurement of Mean Initial Velocity of Ions Desorbed by Carbon-Based SALDI. The DE method is based on the measurement of total flight time (t_{total}) of desorbed ions transmitting from sample plate to detector, which is correlated to a number of parameters, including the initial velocity (υ_0, in ms^{-1}) of desorbed ions, listed in **Equations S.1 – S.4**. These equations have been explicitly derived by Karas and Glückmann [*J. Mass Spectrom.* **1999**, *34*, 467-477] and only a brief description will be given here. In the SALDI-TOF mass spectrometric system operated in a delayed extraction mode, desorbed ions possessing an initial velocity (υ_0) would travel a distance (x) away from the sample plate during a delay extraction period (*t*, in nanosecond scale) without applying electrical potential gradient in the travelling region. The length of distance (x) traveled would determine the magnitude of potential energy of the ions gained in the accelerating region after applying acceleration potentials, and thus affecting the terminal kinetic energies of the desorbed ions, which would finally determine the total flight time of the ions. By measuring the total flight time (t_{total}) of the desorbed ions at a number of different extraction delays (*t*), the initial velocity (υ_0) of the desorbed ions could be determined by a numerical fitting of **Equation S.1**.

$$t_{total} = \frac{\sqrt{2m}}{z}\left(\frac{\sqrt{E_{kin1}} - \sqrt{E_{kin0}}}{U_1} d_1 + \frac{\sqrt{E_{kin2}} - \sqrt{E_{kin1}}}{U_2} d_2\right) + L\sqrt{\frac{m}{2E_{kin2}}} \qquad \textbf{Eqn. S.1}$$

$$E_{kin0} = \frac{1}{2} m v_0^{\,2} \qquad \textbf{Eqn. S.2}$$

$$E_{kin1} = zU_1 - \frac{v_0 t}{d_1} zU_1 + \frac{1}{2} m v_0^{\,2} \qquad \textbf{Eqn. S.3}$$

$$E_{kin2} = zU_2 + zU_1 - \frac{v_0 t}{d_1} zU_1 + \frac{1}{2} m v_0^{\,2} \qquad \textbf{Eqn. S.4}$$

where, *m* is the mass of the ion (in kg), *z* is the charge of ion (in Q). d_1 (0.003 m), d_2

(0.025 m) are the length of the 1st and 2nd ion-accelerating regions, and L (1.125 m) is the length of the flight tube. U_1 (+900 V) is the accelerating potential in the 1st ion accelerating region between the sample plate (+3,000 V) and the 1st ion focusing lens (+2,100 V). U_2 (+14,100 V) is the accelerating potential in the 2nd ion accelerating region between the 1st ion focusing lens (+2,100 V) and the flight tube (-12,000 V). The E_{kin0} is the initial kinetic energy of the desorbed ions with initial velocity at υ_0 as described in **Equation S.2**. The E_{kin1} and E_{kin2} are the terminal kinetic energies of the desorbed ions in the respective 1st and 2nd ion-accelerating regions, as described in **Equations S.3 and S.4**, respectively. In the numerical fitting, d_1 is set as a variable to compensate for the roughness of the sample surface.

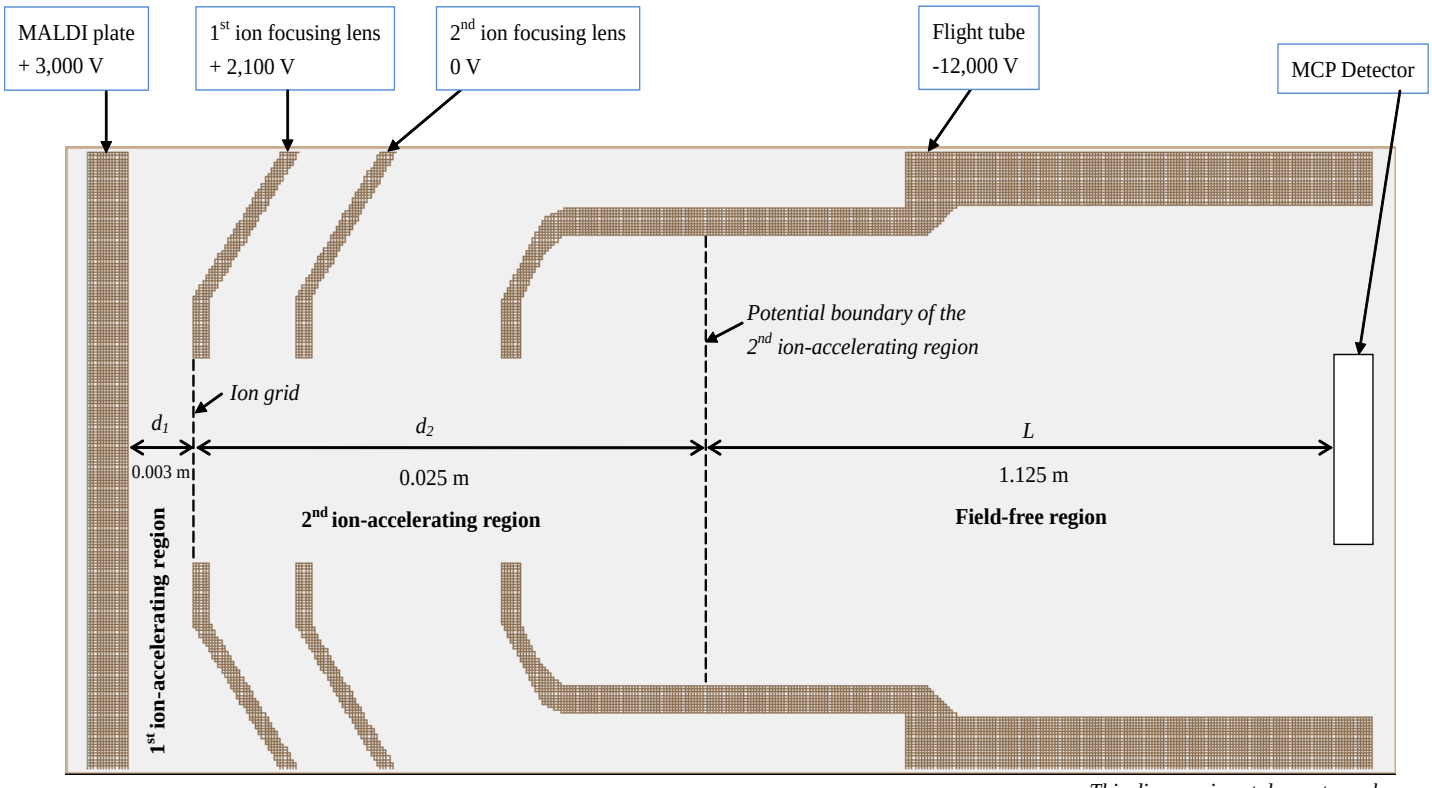

Remarks: The length (d_1) of the 1st ion-accelerating region, well defined by the partition of a potential grid, is 0.003 m. In the absence of the 2nd potential grid, the effective length (d_2) of the 2nd ion-accelerating region was approximated to be 0.025 m by performing an electrical potential simulation using Simion 8.0 (Scientific Instrument Services, Ringoes, NJ) and the value is consistent with that provided by the instrument manufacturer.

Figure S1. Schematic diagram of the Waters micro MX MALDI-TOF mass spectrometric system

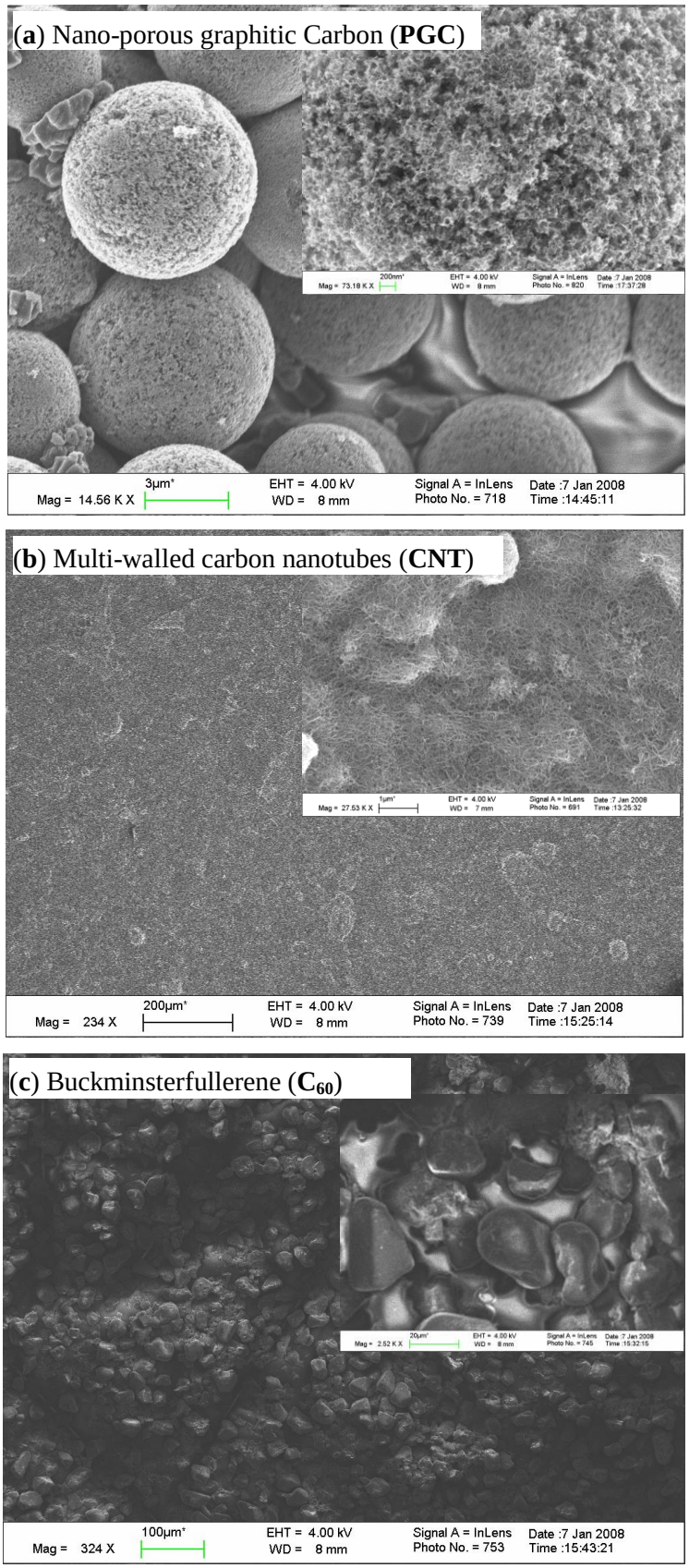

Figure S2. Scanning electron micrographs of (**a**) nano-porous graphitic carbon, (**b**) multi-walled carbon nanotubes, (**c**) buckminsterfullerene, (**d**) non-porous graphite particles, (**e**) highly oriented pyrolytic graphite, and (**f**) nano-diamonds.

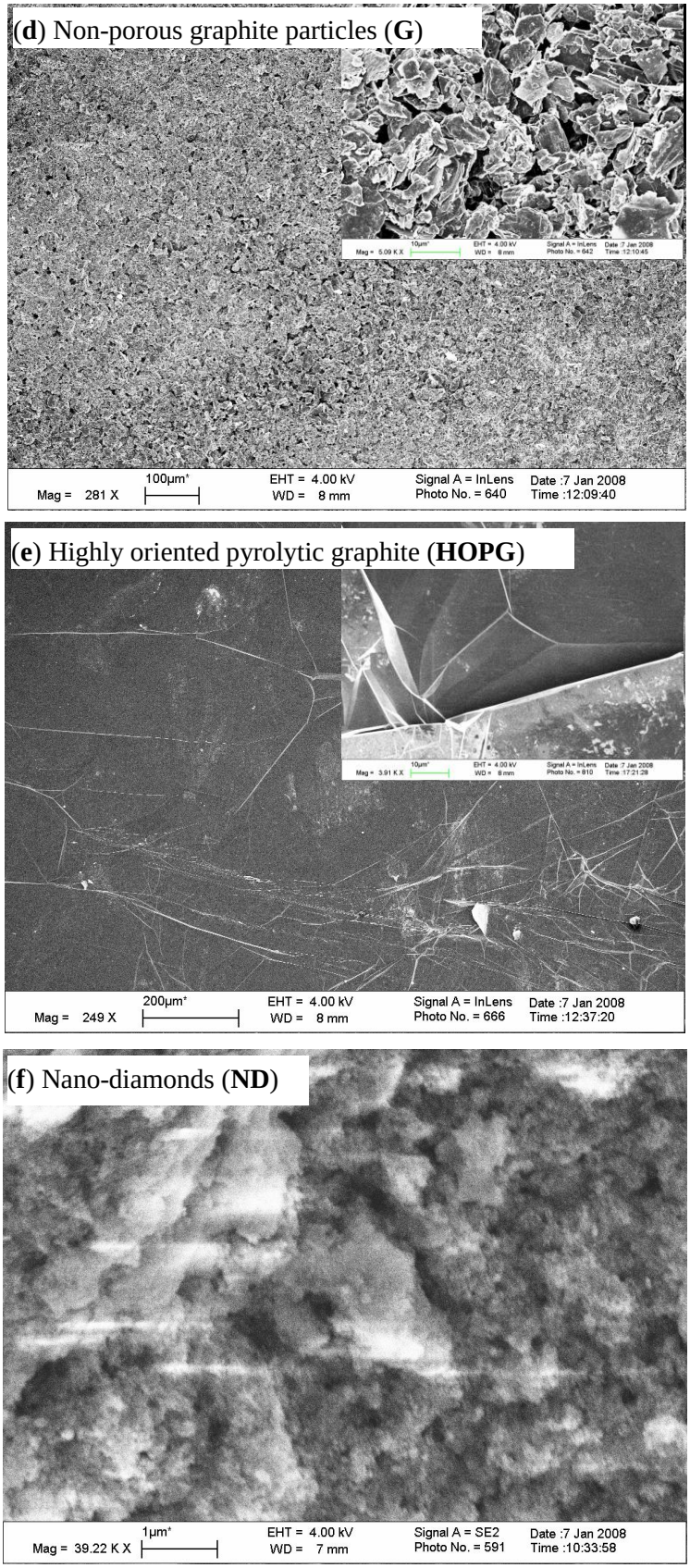

Figure S2. Scanning electron micrographs of (**a**) nano-porous graphitic carbon, (**b**) multi-walled carbon nanotubes, (**c**) buckminsterfullerene, (**d**) non-porous graphite particles, (**e**) highly oriented pyrolytic graphite, and (**f**) nano-diamonds.

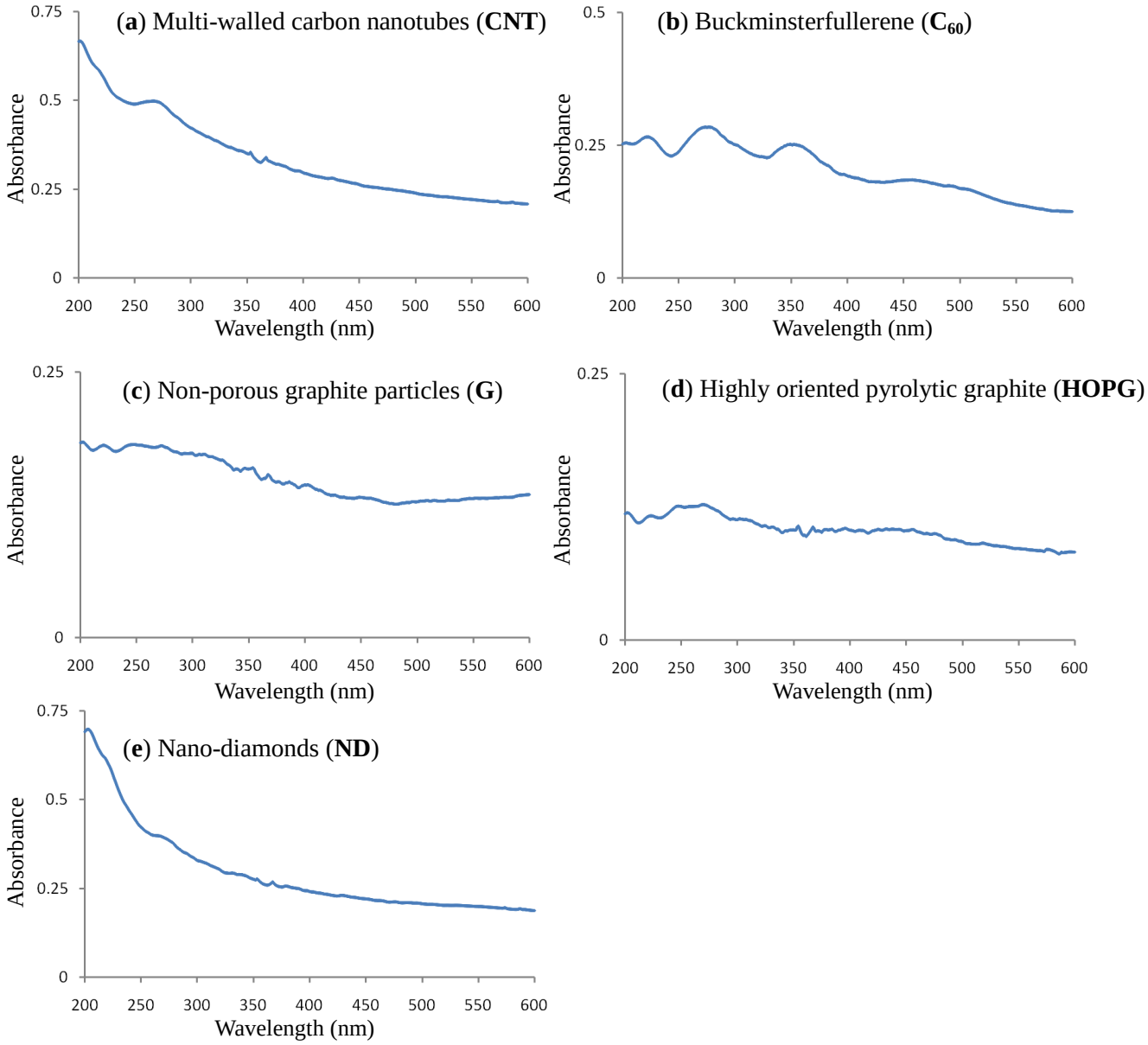

Figure S3. UV-visible spectra of (**a**) multi-walled carbon nanotubes (**CNT**), (**b**) buckminsterfullerene ($\mathbf{C_{60}}$), (**c**) non-porous graphite particles (**G**), (**d**) highly oriented pyrolytic graphite (**HOPG**), and (**e**) nano-diamonds (**ND**). The UV-visible absorbance was measured from a film of the respective carbon substrate. The substrate film was formed by deposition of 200 µL of the respective substrate suspension on a quartz coverslip (25 x 25 x 0.2 mm). **CNT** and **ND** were suspended in dimethylforamide (0.1 mg/ mL). $\mathbf{C_{60}}$ was dissolved in toluene (0.1 mg/ mL). **G** and **HOPG** were suspended in isopropanol (1 mg/ mL). All suspension and solution were sonicated for 30 min before use. The UV-visible absorbance measurements were performed by using a photodiode array spectrophotometer (U-0080D, Hitachi High Technologies, Japan).

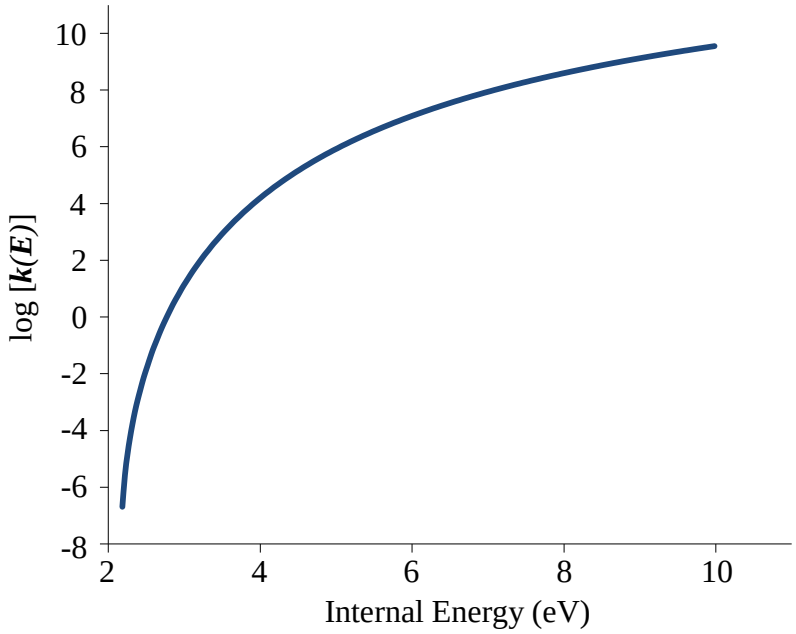

Figure S4. The internal energy dependent dissociation rate coefficient curve of benzylpyridinium ions derived from the RRKM formalism using the Masskinetics program.

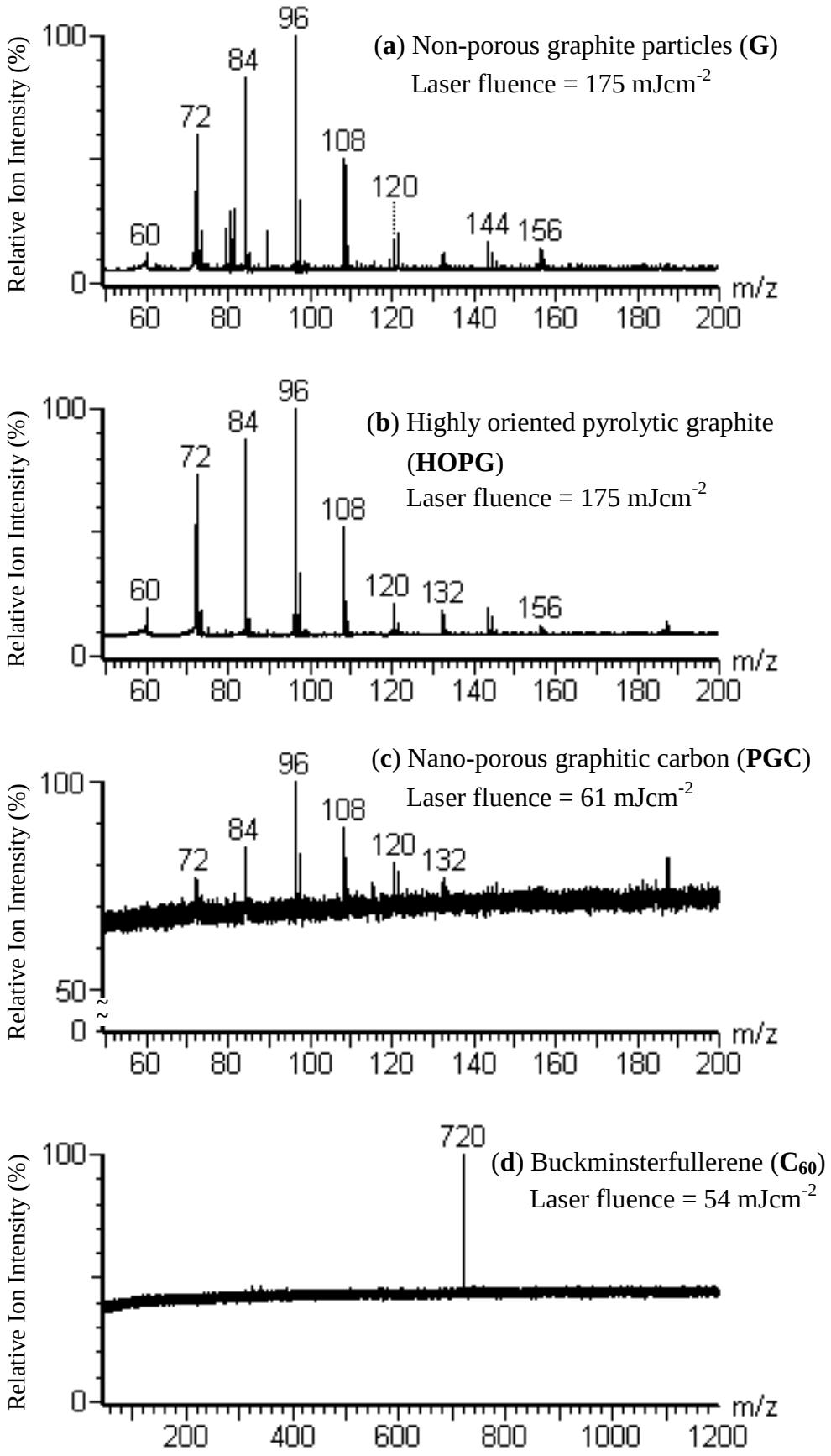

Figure S5. Negative SALDI mass spectra of (**a**) non-porous graphite particles, (**b**) highly oriented pyrolytic graphite, (**c**) nano-porous graphitic carbon and (**d**) buckminsterfullerene.

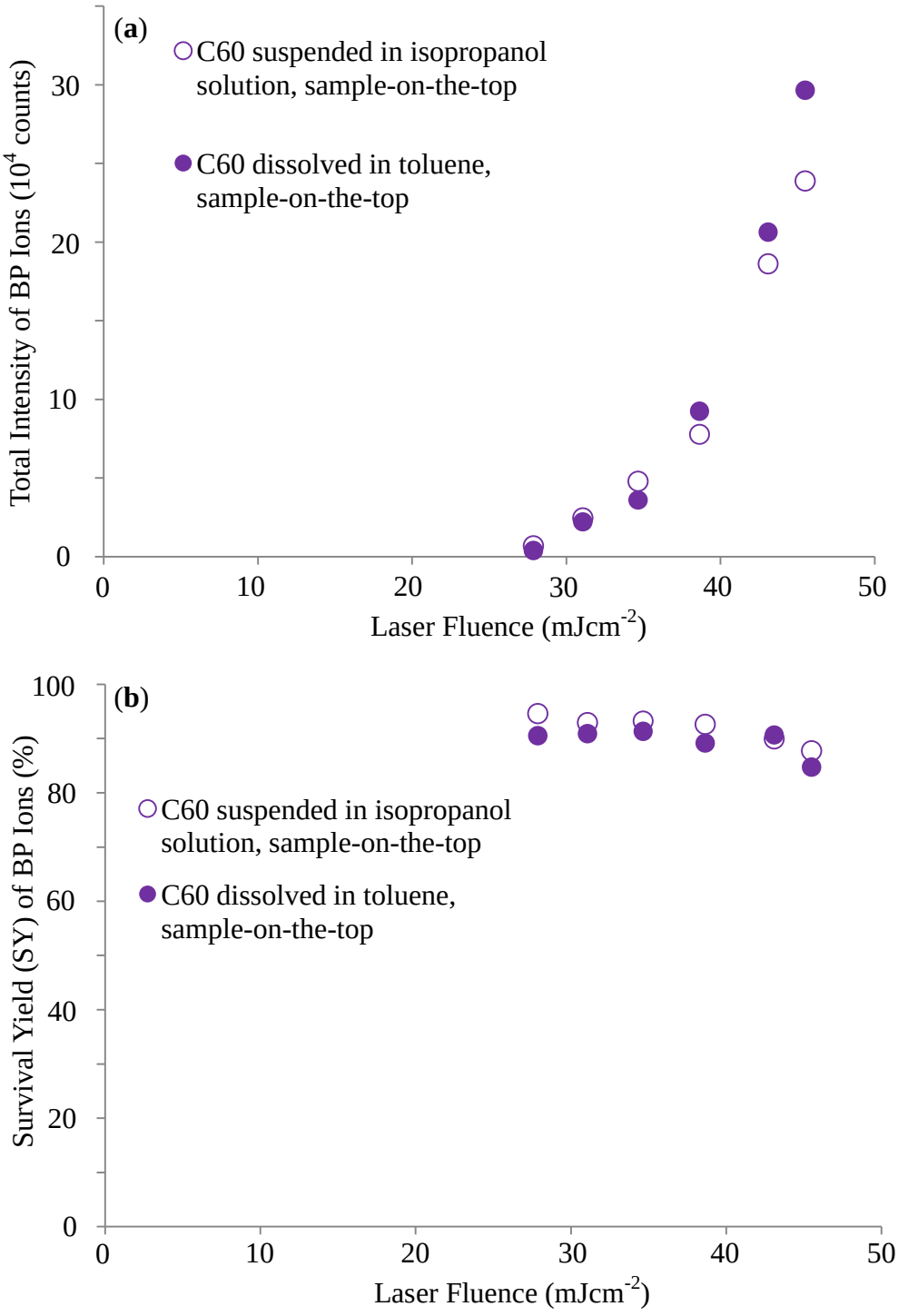

Figure S6. Comparison of (**a**) total intensity and (**b**) survival yield of benzylpyridinium (BP) ions desorbed from buckminsterfullerene ($\mathbf{C_{60}}$) substrate deposited by using (○) $\mathbf{C_{60}}$ suspended in isopropanol solution and (●) $\mathbf{C_{60}}$ dissolved in toluene. The concentration of the $\mathbf{C_{60}}$ suspension (in isopropanol solution) and $\mathbf{C_{60}}$ solution (in toluene) were 4 and 2 mg/mL respectively. All sample spots contained the same amount of $\mathbf{C_{60}}$ (0.03 mg). No conductive tape was used for the sample spot prepared by using $\mathbf{C_{60}}$ dissolved in toluene.

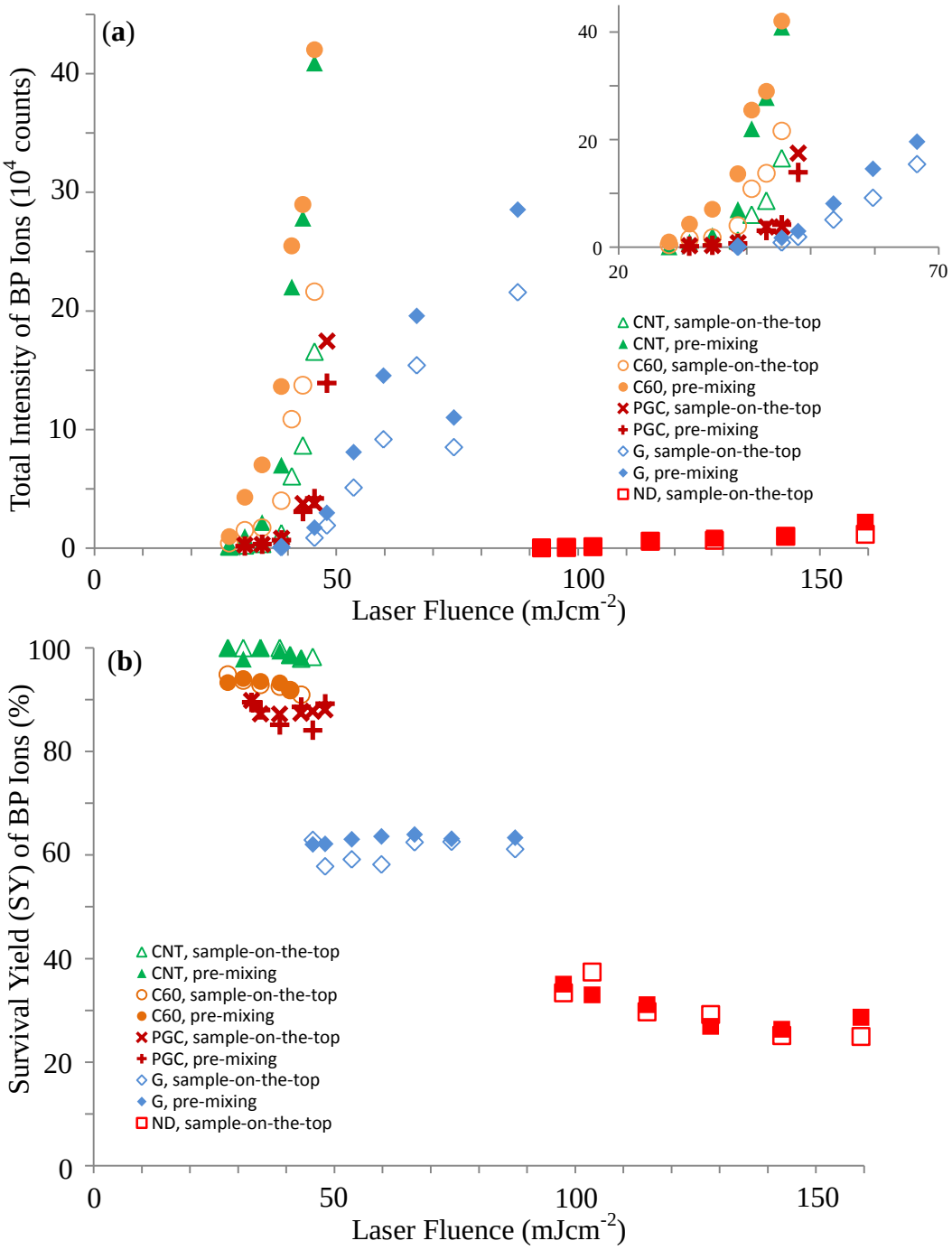

Figure S7. Effect of sample deposition method (sample-on-the-top versus pre-mixing) on (**a**) total intensity and (**b**) survival yield of benzylpyridinium (BP) ions desorbed from various carbon substrates. The total ion intensities are the summation of intensities of BP ion at m/z 170 and the fragment ion at m/z 91. For **CNT** and **PGC**, the pre-mixed solution was prepared by mixing the respective carbon substrates suspension (4 mg/mL) and BP (1 x 10^{-4} M) in a 2 : 1 ratio (v/v). Each sample spot was prepared from a total volume of 4.5 µL of the pre-mixed solution. For **C_{60}**, **G** and **ND,** the sample preparation procedures were similar except that the mixing ratio was changed to 5 : 1 and each sample spot was prepared from a total volume of 9 µL of the pre-mixed solution. (**CNT**: carbon nanotubes, **C_{60}**: buckminsterfullerene, **PGC**: nano-porous graphitic carbon, **G**: non-porous graphite particles, **ND**: nano-diamonds)

Table S1. Survival yield (SY) and extent of internal energy transfer in 4-fluoro-benzylpyridinium and 4-chloro-benzylpyridinium ions generated by the carbon-based SALDI using different carbon substrates.

4-chloro-benzylpyridinium ion, E_0 = 2.04 eV			
Carbon substrates	Survival yield (%)	Internal energy transfer (eV)	Laser fluence ($mJcm^{-2}$)
CNT	96.1 - 75.7	4.41 – 4.96	36 - 54
PGC	92.5 - 87.2	4.59 - 4.75	32 - 54
C_{60}	78.8 - 69.7	4.91 - 5.04	28 - 54
G	67.6 - 56.9	5.07 - 5.18	36 - 54
HOPG	77.2 - 74.1	4.94 - 4.98	92 - 109
ND	29.9 - 28.3	5.45 - 5.47	92 - 116

4-fluoro-benzylpyridinium ion, E_0 = 2.05 eV			
Carbon substrates	Survival yield (%)	Internal energy transfer (eV)	Laser fluence ($mJcm^{-2}$)
CNT	96.1 - 71.2	4.58 - 5.23	36 - 54
PGC	92.0 - 87.3	4.79 - 4.94	32 - 54
C_{60}	80.3 - 69.8	5.09 - 5.25	28 - 54
G	66.3 - 56.0	5.30 - 5.42	36 - 54
HOPG	73.7 - 73.0	5.19 - 5.21	92 - 109
ND	32.5 - 29.0	5.67 - 5.70	92 - 116

[a] **CNT**: Carbon nanotubes, **PGC**: Nano-porous graphitic carbon, **C_{60}**: Buckminsterfullerene, **G**: Non-porous graphite particles, **HOPG**: Highly oriented pyrolytic graphite, **ND**: Nano-diamonds

Table S2. Mean initial velocities of benzylpyridinium ions generated by the carbon-based SALDI using different carbon substrates, measured by the delayed extraction method.

Carbon substrates[a]	Mean initial velocity (ms^{-1})	Laser fluence ($mJcm^{-2}$)
CNT	1130 - 1250	30 - 43
PGC	1200 - 1230	34 - 54
C_{60}	1260 - 1330	30 - 43
G	1250 - 1320	43 - 68
HOPG	1090 - 1280	61 - 109
ND	1290 - 1420	68 - 109
CHCA[b]	1270 - 1350	38 - 54

[a] **CNT**: Carbon nanotubes, **PGC**: Nano-porous graphitic carbon, **C_{60}**: Buckminsterfullerene, **G**: Non-porous graphite particles, **HOPG**: Highly oriented pyrolytic graphite, **ND**: Nano-diamonds

[b] Mean initial velocity of BP ions generated by MALDI using CHCA as the matrix was measured as the reference.